STUDY OF THE PHOTOLUMINESCENCE OF NANOCRYSTALS USING ULTRAFAST UPCONVERSION

by

D. Lawrence Whipple

A senior thesis submitted to the faculty of

Brigham Young University

in partial fulfillment of the requirements for the degree of

Bachelor of Science

Department of Physics and Astronomy

Brigham Young University

December 2006

BRIGHAM YOUNG UNIVERSITY

DEPARTMENT APPROVAL

of a senior thesis submitted by

D. Lawrence Whipple

This thesis has been reviewed by the research advisor, research coordinator, and department chair and has been found to be satisfactory.

Date	Brett C. Hess, Advisor
Date	Eric G. Hintz, Research Coordinator
Date	Scott D. Sommerfeldt, Chair

ABSTRACT

STUDY OF THE PHOTOLUMINESCENCE OF NANOCRYSTALS

USING ULTRAFAST UPCONVERSION

D. Lawrence Whipple

Department of Physics and Astronomy

Bachelor of Science

We apply the method of sum generation upconversion to the photoluminescence to study the dynamics of type Cadmium Telluride nanocrystals. Our sum generation technique uses type1 phasematching with a nonlinear beta-barium borate crystal. We maximize the efficiency and give our best values.Three measures are incorporated to reduce stray photons due to the second harmonic generation of the excitation laser created in the crystal: noncollinear geometry, short pass filters and a monochromator. Applying this upconversion method to the photoluminescence of nanocrystals shows the rapid rise in luminescence following the integrated excitation pulse and its slow decay rate due to the to the decrease in carrier population. This technique allows us to observe the excitation lifetimes and the relaxation rate of carriers at the high energies.

ACKNOWLEDGMENTS

I would like to thank my advisor Brett C. Hess for his tremendous knowledge and insight in this area. I would also like to thank Jean-Franscois van Huele for his help and feedback in writing my thesis.

Contents

Table of Contents vii

List of Figures ix

1 Introduction 1

2 Nanocrystals 3
- 2.1 Nanocrystal . . . 3
- 2.2 Particle synthesis . . . 4
- 2.3 Properties of interest . . . 4
- 2.4 Photoluminescence in nanocrystals . . . 5

3 Upconversion theory 7
- 3.1 Nonlinear optics . . . 7
- 3.2 Sum frequency generation . . . 8
- 3.3 Phase matching . . . 9
- 3.4 The uniaxial crystal method . . . 10

4 Upconversion procedure 13
- 4.1 Photoluminescence technique . . . 13
- 4.2 Our procedure . . . 15
- 4.3 Results . . . 18
- 4.4 Conclusion . . . 20

Bibliography 23

A Finding θ_{oa} 25

B Maple for finding θ_{oa} 29

Index 45

List of Figures

3.1 Sum Generation 9
3.2 Electron in crystal lattice 11
3.3 Uniaxial Polarizations 12

4.1 Lab Layout 16
4.2 Filter 17
4.3 Photocathode sensitivity 17
4.4 PL dynamics 19

B.1 PL dynamics 30
B.2 PL dynamics 31
B.3 PL dynamics 32
B.4 PL dynamics 33
B.5 PL dynamics 34
B.6 PL dynamics 35
B.7 PL dynamics 36
B.8 PL dynamics 37
B.9 PL dynamics 38
B.10 PL dynamics 39
B.11 PL dynamics 40
B.12 PL dynamics 41
B.13 PL dynamics 42
B.14 PL dynamics 43

Chapter 1

Introduction

Semiconducting NanoCrystals (NC) such as Cadmium Telluride (CdTe) have received attention recently because of their unique optical and electronic properties stemming from quantum confinement. Their tunable optical properties and strong nonlinear optical response make them ideal for building future optoelectronic devices.

The band-edge dynamics of the electron-hole pair or exciton are the operating parameters of these devices. Therefore understanding the dynamics of the exciton relaxation pathway is critical to the design process. Band-edge dynamics are explained as electrons in the valence band being excited into the conduction band by absorption of a photon of appropriate energy levels leaving a positively charged hole in the valence band.

Time resolved luminescence spectroscopy has provided tremendous understanding of this behavior in NC. This method allow us to study the bulk dynamics of excitons with excellent time resolution. Achieving good time resolution is done by using nonlinearity induced by laser pulses as a timed gate for the NC luminescence. Developing a method which can take full advantage of the ultrashort pulsewidth of the lasers is the latest focus.

The purpose of this paper is to discuss the various steps of frequency mixing for time resolved luminescence spectroscopy. We focus entirely on the technique of sum generation frequency mixing also known as upconversion.

The paper is organized as follows. An overview of NC and their properties is discussed in chapter two. Basic concepts of sum generation for frequency mixing are reviewed in chapter 3. A brief explanation of the standard method of upconversion is discussed in chapter four as well as our techniques for optimization of the luminescence signal. Our data using this technique with CdTe NC and an explanation of our results end chapter four.

Chapter 2

Nanocrystals

2.1 Nanocrystal

Crystalline inorganic solids are electronically categorized as metals, semiconductors, and insulators. These solids have atomic orbital's that overlap to give almost continuous electronic energy levels or bands. Metals have partially filled conduction bands. Semiconductors have filled valence bands and a mostly empty conduction band separated by a band-gap energy (Eg). Insulators have the same electronic structure as semiconductors except with a larger Eg. If the size of the crystalline inorganic solid is on the order of nanometers they are referred to as NanoCrystals (NC).

NC are studied for many reasons including their use as semiconductors where the electron-hole recombination process can be controlled by the particle size. An electron-hole or hole is the absence of an electron from the otherwise full valence band. The electron-hole pair is referred to as an exciton. An exciton occurs when the electron is excited from the valence band into the conduction band through absorption of a photon leaving an electron hole.

2.2 Particle synthesis

The most common technique for nanocrystal synthesis is bottom up synthesis . This is creating the desired type of particle from elemental precursors in a chemical reaction. The precursor sources are varied to optimize reaction and growth. These sources are usually injected into solvents or amines, depending on the modeled prep., at the temperature of desired growth size.

These solvents and amines acted as capping agents. Capping stops particle growth. Capping also interferes with the recombination of electron-hole pairs and can shift the Eg. With small particles, capping can shift the Eg to lower energy. Also, impurities can cause trapped states in which electron-hole pairs do not recombine. This can reduce or oxidize the particles at the surface. Capping with a shell of higher-band-gap energies can eliminate trapped states.

2.3 Properties of interest

The electronic properties of a material change as a consequence of reducing its size and dimensionality. In nanometer size crystals, transitions from the bulk band structure now occur in individual localized energy levels. This is because the density of states and spatial length of the electronic motion are reduced with decreasing size. The system's boundaries now determine the energy eigenstates. However this also means that surface defects are more important

For a typical semiconductor the calculated electron-hole pair, or exciton, spatial separation is 1-10 nm. If the particle is in this size range it confines the exciton similar to the "particle in a box" representation. The electron is delocalized over the whole particle and the electron hole is localized at the center. Therefore the Eg is dependent on particle size allowing for control of the Eg by the particle size. From the small

particle size and its quantized electronic states, a large amount of energy is required to add a single electron. Electron flow through a NC can therefore proceed only one electron at a time. This causes a blockade effect. Particles with such properties could be used for nanoscale gates, for example, in quantum computing.

Metallic types of NC's are of particular interest because of their magnetic properties. This allows for utilization of the electron spin states. Conventional electronic devices rely on the transport of electrons. Physicists are now trying to use the spin of the electron rather than its charge to create devices which will be smaller, and more robust than those currently made of silicon chips and circuit elements.

2.4 Photoluminescence in nanocrystals

PhotoLuminescence (PL) is explained as the recombination of the electron-hole pair. Incident photons are absorbed by the electrons through inter-band transitions. The photon energy excites these electrons into states above the Fermi level in the sp-conduction band leaving positively charged holes. Both electrons and holes relax by scattering with phonons through the lattice and then recombine radiating luminescence.

The recombination processes happens as the exciton is allowed to travel in the spatial boundaries of the NC. Therefore, the electron-hole wave function interactions depend on NC size. For smaller NC's the increased exciton wave function overlap with surface states leads to faster decay than larger NC's, even though with increasing NC size, the valence and conduction bands become closer in energy. This size dependence is seen for the band-edge emissions.

Chapter 3

Upconversion theory

3.1 Nonlinear optics

Nonlinear optics is the study of the response of the optical properties of a medium in the presence of light. It is considered nonlinear when the response to a medium is not proportional to the input optical field.

For small inputs most systems respond with optical linearity. Optical linearity is where the polarization $P(t)$ of a system depends upon the strength $E(t)$ of the field linearly by the relation

$$P(t) = \chi(1)E(t). \tag{3.1}$$

Where $\chi(1)$ is known as the linear susceptibility.

Under extreme inputs the optical response for some mediums is described by expressing $P(t)$ as a power series in the field strength $E(t)$ as

$$P(t) = \chi(1)E(t) + \chi(2)E2(t) + \chi(3)E3(t) + ... \tag{3.2}$$

$$= P1(t) + P2(t) + P3(t) + ... \tag{3.3}$$

Where the quantities $\chi(2)$ and $\chi(3)$ are the second and third order nonlinear optical susceptibilities. Usually laser intensities are required to create such nonlinear responses.

This nonlinear response of a medium to an intense laser field causes the polarization of the medium to have new frequency components that are not part of the original incident field. These new frequency components of the polarized medium act as sources for new frequency components of the resulting electromagnetic field. For a complete explanation of how Maxwell's equations describe the generation of these new components of the field see Boyd *et al*[1].

3.2 Sum frequency generation

Lets consider two input fields of frequency ω_1 and ω_2. Because the atomic response is nonlinear, each atom will oscillate with a dipole moment at each frequency ω_1 and ω_2. The atom radiates at the sum of these frequencies in a dipole radiation pattern. In an large number N of atomic dipoles, the atoms oscillate with a phase determined by the phases of the original incident field. By matching these dipole phase's, a well defined beam is created as the field radiates constructively.

If we allow one of the input fields (say ω_1), to be weak and the other field (say ω_2), to be strong, this process would lead to an upconversion of the weak beam into a stronger frequency ω_3 by the mixing of the frequencies ω_1 and ω_2 as shown in Fig. 3.1.

We use this process of upconversion to convert the information bearing beam in our experiment to a higher frequency since optical frequency waves are detectable with greater sensitivity.

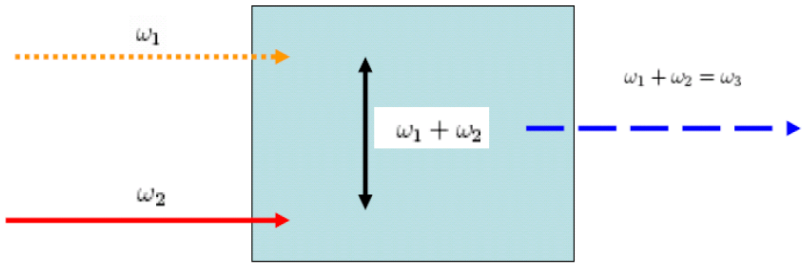

Figure 3.1 The upconversion of a weak (ω_1) frequency into a stronger one (ω_3) through sum generation.

3.3 Phase matching

When the medium reacts as a phased array of dipoles, phase matching occurs. As a result, the strength of the electric field radiation is N times larger in the forward direction, hence, the intensity is N^2 larger.

For sum frequency generation the intensity of the generated beam at frequency

$$\omega_1 + \omega_2 = \omega_3 \tag{3.4}$$

varies with

$$\triangle k = k_1 + k_2 - k_3 \tag{3.5}$$

according to

$$I_3 = I_3 max \frac{sin^2(\triangle k \frac{L}{2})}{(\triangle k \frac{L}{2})^2} \tag{3.6}$$

Therefore a decrease in the efficiency of sum frequency generation occurs when $\triangle k \neq 0$.

Phase matching ($\triangle k = 0$) is difficult to achieve because the refractive index of materials leads to dispersion. Dispersion results with the refractive index becoming an increasing function of frequency. Therefore the sum frequency generation becomes more complicated. The condition becomes

$$n_1\omega_1 + n_2\omega_2 = n_3\omega_3 \tag{3.7}$$

and so the summing of Eq (3.1) cannot be achieved without the use of additional methods. The most common method used to achieve phase matching is to use the birefringent property of crystals.

3.4 The uniaxial crystal method

In a crystal the connection between P and E are not necessarily linear. There are asymmetries caused by the electrons being bound in the lattice by different strengths in different dimensions as shown in Fig. 3.1.

Therefore the energy associated with the s and p polarized light follow different paths. As a result, the refractive index of the crystal is dependent on the direction of the polarization of the optical radiation. This property is known as birefringence.

Phase matching through crystals is achieved when the highest frequency wave in Eq. (3.7) is polarized in the direction of the lowest of the two refractive indexes. There are two choices for the polarizations of the lower-frequency waves defined as Type-1 phase matching and Type-2 phase matching. Type-1 occurs when the two lower frequency waves have the same polarization. Type-2 is where they are orthogonal. We choose Type-1 since it is relatively easier to achieve.

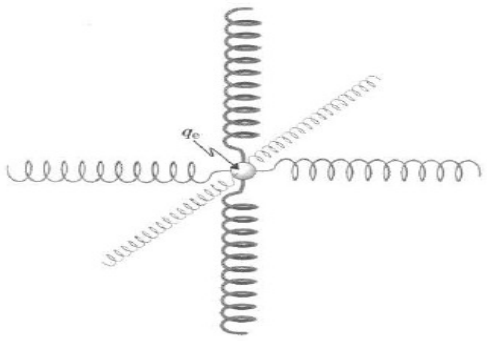

Figure 3.2 An electron bound in a crystal lattice[3].

By controlling the refractive indexes of each of the three frequencies, the phase matching condition is met. This can be done through the method of angle tuning.

Angle Tuning involves precise angular orientation of a uniaxial crystal with respect to the direction of the incident light.

Uniaxial crystals are characterized by the optical axis, ordinary (no) and extraordinary (ne). Ordinary is where the polarization is perpendicular to the plane containing the optical axis and the k vector. Extraordinary is where the is polarization is in the plane as shown in Fig 3.2.

Therefore the index of extraordinary (ne) will depend on the angle θ between the optical axis and k by the relation

$$\frac{1}{ne(\theta)^2} = \frac{sin(\theta)^2}{ne^2} + \frac{cos(\theta)^2}{no^2} \tag{3.8}$$

By adjusting the angle θ to achieve the value $ne(\theta)$ for which $\triangle$k=0, phase matching can be accomplished. The condition becomes

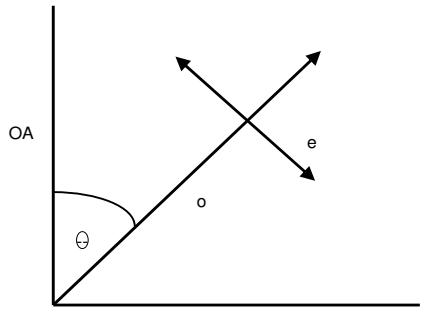

Figure 3.3 The optical axis with ordinary (no) and extraordinary (ne) polarizations. Ordinary light is polarized perpendicular to the plane containing the optical axis and the k vector. Extraordinary light is polarized in the plane.

$$ne(2\omega, \theta) = no(\omega) \tag{3.9}$$

or

$$\frac{sin^2(\theta)}{ne(2\omega)^2} + \frac{cos^2(\theta)}{no(2\omega)^2} = \frac{1}{no(\omega)^2} \tag{3.10}$$

.....solving to give

$$sin(\theta) = \sqrt{\frac{\frac{1}{no(\omega)^2} - \frac{1}{no(2\omega)^2}}{\frac{1}{ne(2\omega)^2} - \frac{1}{no(2\omega)^2}}} \tag{3.11}$$

Which gives the alignment angle θ of the crystal for perfect phase matching.

Chapter 4

Upconversion procedure

4.1 Photoluminescence technique

Optical properties of NC's are closely related to size-induced changes in the electronic structure. These optical properties directly reflect the size-dependent energy structure of the particle. Therefore optical methods such as luminescence spectroscopy can reveal the dynamic behaviors of the physical systems of NC. By using time resolved spectroscopic methods such as up-conversion, the behaviors of the electrons in NC are observed.

The technique of upconversion uses nonlinearity caused by ultrafast laser pulses as a timed light gate for luminescence. These laser pulses are generated by a mode locked laser. By constructive interference, a short pulse is formed when many longitudinal modes are held in phase in a laser cavity. These extremely short pulse durations allow for the creation, detection and study of very short-lived energy differences between allowed electron transition states as well as excited state lifetimes. This information will help us to understand the localizations of the electron states, alignment of energy levels, and the influence of excess charge in the NC.

Using ultra-fast laser pulses (100 fs), an excitation pulse is sent into the NC sample. The excitation of the electrons in the sample by the pulse leads to a perturbation of the electron distribution in the crystal creating exciton's or electron-hole pairs. These exciton's scatter and recombine, emitting PL. The PL is time resolved when the luminescent and probe pulse wavelengths of light are focused onto a nonlinear crystal which is oriented at the phase matching angle with respect to both beams. During the time that the PL and probe beams are both present at the crystal, photons with energy equal to the sum of the two separate photon energies are created.

Frequency mixing acts as a light gate which allows us time resolution comparable to pulse width. Time resolution of PL is obtained by setting the crystal angle and the monochromator wavelength at the predicted values for upconverted PL and changing the delay of the probe beam at the crystal. By sending the probe beam through an optical delay line, the luminescence intensity is shown in controlled time-slices.

Zero time delay precision is essential in this technique. This provides an accurate measure of the time resolution for the upconverted signal. An accurate zero time can be determined by obtaining a cross correlation trace between the scattered pump beam light from off the sample and the delayed probe beam at the nonlinear crystal used for sum generation. The crosscorrelation for our experiment is shown in fig.(4.2) and the typical resolution for our experiment is the FWHM value of this peak.

The overall accuracy of the time resolution depends on the strength of the PL signal and the sensitivity of the detectors. The unpolarized PL is typically only about 50 percent phase matched since phase matching occurs for a narrow band of wavelengths centered at the wavelength delay determined by the phase matching angle. Therefore maximizing signal to noise ratios are critical to detect the faint PL signal. If the PL is close to the second harmonic generation of the pump laser then the this signal may be detected instead. So signal to noise is improved by eliminating

these stray photons. Also signal to noise is partially determined by the dark current of the detector and the fluctuations in the laser.

Changing the angle of incidence of the PL also leads to deviations from the perfect phase matching. Since luminescence is emitted in all directions from the excited spot the efficiency of our technique is reduced if the angle of acceptance on the nonlinear crystal is smaller than the luminescence solid angle of divergence. Therefore the angle of acceptance of luminescence by the nonlinear crystal is important for this experiment.

4.2 Our procedure

Ultra-fast PL dynamics were observed using sum generation up-conversion technique. As shown in Fig. 4.1, the excitation source was a frequency-doubled Ti:sapphire laser. The source is sent through a beam splitter to generate the pump and probe pulses. Pump pulses has time duration of 100 fs and a wavelength of 400nm. The pump pulse is then sent through a frequency chopper at 279Hz enabling the detection of the PL through a lock in amplifier set to detect pulses at that frequency. The beam is then focused onto our NC sample of CdTe in solution. Upconverted emission was resolved by the phase matching process where the PL from the sample is gathered and both the PL and probe femto-second pulse are focused onto a nonlinear beta-barium borate crystal (BBO) set at the appropriate phase matching angle to produce light at the sum frequency. This sum frequency light is predicted by the simple relation

$$\frac{1}{\lambda_{uv}} = \frac{1}{\lambda_{pl}} + \frac{1}{\lambda_{pb}} \tag{4.1}$$

and found to be at 342nm where the PL from our NC sample is expected to be 600nm (λ_{pl}) and the probe beam was 800nm (λ_{pb}). The phase matching angle was

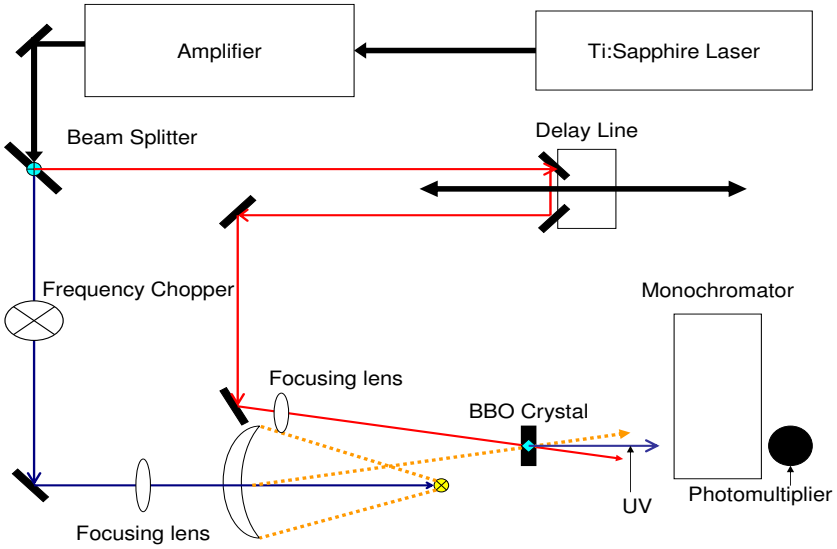

Figure 4.1 Simplified layout of our Upconversion lab.

predicted by eq. 3.11 and found to be -52 degrees from normal. The upconverted signal is passed through a monochromator and then detected by a photon counting photo multiplier with a low enough dark current to be considered negligible. The PL behaviors are observed by delaying the probe pulse relative to the PL pulse. Changing the time delay between the pump and the probe laser pulses was done with the optical delay line and maps out the decay rate of the PL at 1ps resolution time slices. Time resolution is possible since the up-conversion process takes place only during the presence of both the PL and probe pulse in the BBO crystal. Time resolution of our system is determined by the laser pulse width and the group velocity dispersion mismatch between the pump pulses and PL. Our laser pulse width is around 100 fs.

To improve signal to noise we use noncollinear geometry as shown in Fig. 4.1, meaning the PL and probe beams are not parallel into the crystal. Using this non-collinear geometry reduces the stray photons due to the Second Harmonic Generation

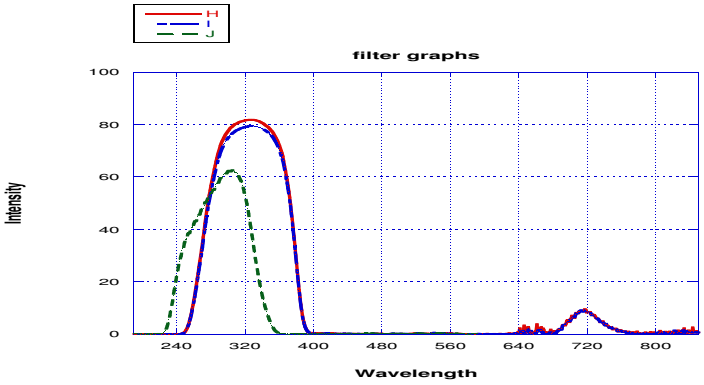

Figure 4.2 Short pass filters used with photomultiplier.

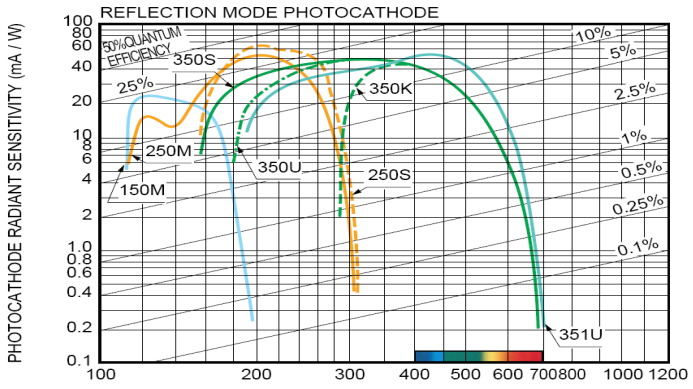

Figure 4.3 Photocathode or electron tube sensitivity in the UV range.

(SHG) of the laser in the crystal by increases the angular spread between the sum and SHG beams. Stray photons are also decreased with the use of a monochromator.

Stray photons are also eliminated by passing upconverted light through three short pass filters to filter out residual excitation light. The varying wavelength cutoffs are seen in the fig.(4.2). We also used a photomultiplier with a photocathode of UV radiant sensitivity seen in Fig. 4.3.

Taking these measures to eliminate stray photons insures us increases in the dynamic range of the sensitivity of the upconversion wavelength predicted by Eq.(4.1).

4.3 Results

Fig. 4.2 shows the time evolution of the up converted PL signal of type CdTe NC's at a wavelength determined by Eq.(4.1) for different time delays with the crosscorrelation indicating zero time and the temporal resolution of about 1ps. The rise and decay rates indicate the time scale of the NC relaxation. The rapid rise in luminescence following the integrated excitation pulse is observed. This shows the excitation lifetimes and the relaxation rate of carriers at the high energies.

This risetime for the PL is around 10ps and is an indication of the time taken for the excited carriers to cool down to the NC lattice temperature. The Eg was determined from the wavelength emitted from the NC sample. Our CdTe emitted an orange luminescence which we approximated to be around 600nm. Using Eq.(4.1) we predict the sum frequency wavelength. Once the actual sum frequency is detected (determined by the PL peak), we solve the exact luminescence wavelength with Eq.(4.1) which enables us to arcuately determine the Eg.

The actual PL peak corresponds to an electron temp higher than the lattice temp. The initial excess in energy given to an exciton pair is the difference between the ex-

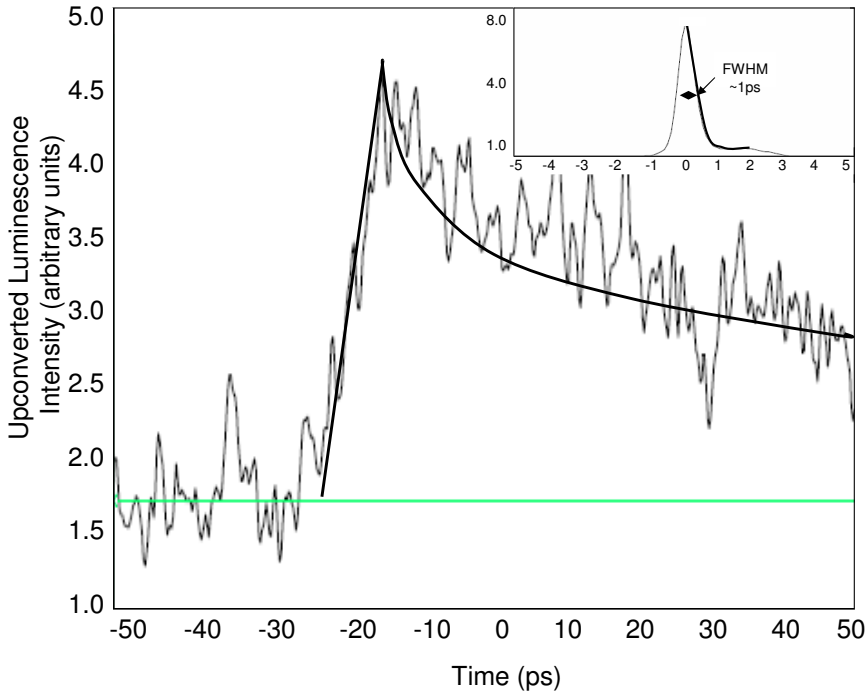

Figure 4.4 Ultra fast band edge emission (PL) from CdTe NC samples by 400nm femtosecond pulses. The smooth curve is an exponential fit. Inset: Our crosscorrelation scan defining our resolution to be about 1ps.

citation pulse energy and the Eg of the NC and is generally explained by carrier relaxation and surface trapping and by the NC lattice relaxation. The PL is interpreted to be due to the radiative recombination of exciton states interior to the NC. After the PL intensity rises to a maximum it slowly decays due to the decrease in carrier population through thermal losses until the bandgap and then through the bandgap by radiative losses (PL). A full spectrum of the ultrafast PL (not shown) reflects the interior states energy distribution. The steep rise in Fig. 4.2 indicates that the states from in the NC from where the PL originates are populated within our laser pulse width time of 100fs after the excitation.

The smooth curve is a result of fitting the experimental data with an exponential decay function with the time response of the upconversion. The largest amplitude of decay (2ps) is attributed to the recombination from the band-edge states which falls off sharply. The longer lived component of decay of the PL emission is due to the dark exciton effect. The dark exciton effect is the exciton thermalization to the lowest quantum state which is optically forbidden. However, a portion of the excitons can relax to a long lived triplet state and recombine through a phonon assisted momentum conserving transition where it briefly enters a higher energy state to an optically allowed transition.

4.4 Conclusion

Femto-second upconversion spectroscopy has been utilized to probe the dynamics of photogenerated excitons in CdTe NC. We attribute the steep PL decay to the recombination from the band-edge states. The longlived PL decay to is explained as dark exciton relaxation from triplet states to the ground state. We have shown the upconversion method as a useful basis for observing excited state dynamics. However

it is complicated by many contributions to the signal. Overall the arrangement is good for obtaining time resolved spectra with excellent time resolution and a capability of determining an accurate zero time delay.

Bibliography

[1] R. W. Boyd, *Nonlinear Optics*, 2nd ed. (Academic Press, California , 2003), p. 80-94.

[2] Y. R. Shen, *The Principles of Nonlinear Optics*, 1st ed. (Wiley, Canada , 1984), p. 67-74.

[3] J. Peatross and M. Ware,*Physics of Light and Optics*, 1st ed. (Brigham Young University, Utah , 2006), p. 93-96.

[4] J. Shaw, "Ultrafast luminescence spectroscopy using sum frequency generation," Journal of Quantum Electronics **24,** 276–288 (1988).

[5] D. F. Underwood, T. Kippeny, and S. J. Rosenthal"Ultrafast Carrier Dynamics in CdSe Nanocrystals Determined by Femtosecond Flourescence Upconversion Spectroscopy," J. Phys. Chem. **105,** 436–443 (2000).

Appendix A

Finding θ_{oa}

Using the equation

$$\frac{n_o(\lambda_{pl})}{\lambda_{pl}}\hat{e}_1 + \frac{n_o(\lambda_p)}{\lambda_p}\hat{e}_2 = \frac{n_{uv}(\theta_{oa})}{\lambda_{uv}}\hat{e}_3 \tag{A.1}$$

where

$$n_{o_i} = \sqrt{2.7359 + \frac{0.01878}{\lambda_i^2 - 0.01822} - 0.01354\lambda_i^2} \tag{A.2}$$

for BBO,

we solve for the angle θ_{oa} by taking the magnitudes (LHS,RHS) of each side and letting maple determine the angles.

The Left Hand Side (LHS) of the equation becomes

$$\sqrt{(\frac{n_{o_p}\cos(\theta_p)}{\lambda_p} + \frac{n_{o_{pl}}\cos(\theta_{pl})}{\lambda_{pl}})^2 + (\frac{n_{o_p}\sin(\theta_p)}{\lambda_p} + \frac{n_{o_{pl}}\sin(\theta_{pl})}{\lambda_{pl}})^2} \tag{A.3}$$

where $\lambda_p = 800$nm, $\lambda_{pl} = 600$nm and n_{o_p}, $n_{o_{pl}}$ were giving values according to eq. 3.13. For our noncollinear setup, $\theta_p = 0$ and $\theta_{pl} = 6.84$rad reducing the LHS to

$$\sqrt{(\frac{n_{o_p}}{\lambda_p} + \frac{n_{o_{pl}}\cos(\theta_{pl})}{\lambda_{pl}})^2 + (\frac{n_{o_{pl}}\sin(\theta_{pl})}{\lambda_{pl}})^2} \tag{A.4}$$

To solve the Right Hand Side (RHS) we make use of eq. 3.8

$$\frac{1}{n_{uv}^2} = \frac{\sin(\theta_{oa})^2}{n_{e_{uv}}^2} + \frac{\cos(\theta_{oa})^2}{n_{o_{uv}}^2} \tag{A.5}$$

where

$$n_{e_{uv}} = \sqrt{2.3753 + \frac{0.01224}{\lambda_{uv}^2 - 0.01667} - 0.01516\lambda_{uv}^2} \tag{A.6}$$

with $n_{o_{uv}}$ given by eq. 3.13 and $\lambda_{uv} = 342$nm.

Using Maple to solve for $n_{uv}(\theta_{oa})$ in eq. 3.12 gives

$$n_{uv}(\theta_{oa}) = \frac{1.0000e^5}{\sqrt{2.29134566e^8\sin(\theta_{oa}) + 5.864536693e^9}} \tag{A.7}$$

making the RHS of eq. 3.12

$$\sqrt{(\frac{\frac{1.0000e^5}{\sqrt{2.29134566e^8\sin(\theta_{oa})+5.864536693e^9}}}{\lambda_{uv}})^2} \tag{A.8}$$

Therefore the equation to solve for θ_{oa} becomes

$$\sqrt{(\frac{n_{o_p}}{\lambda_p} + \frac{n_{o_{pl}}\cos(\theta_{pl})}{\lambda_{pl}})^2 + (\frac{n_{o_{pl}}\sin(\theta_{pl})}{\lambda_{pl}})^2} = \frac{\frac{1.0000e^5}{\sqrt{2.29134566e^8\sin(\theta_{oa})+5.864536693e^9}}}{\lambda_{uv}} \tag{A.9}$$

and solving for θ_{oa} can only be done numerically (see appendix B).

Appendix B

Maple for finding θ_{oa}

Collinear Type 1

```
> restart;with(ListTools):with(plots):
Warning, the name changecoords has been redefined

>
> no:=L-> (2.7359+0.0187e6/(L^2-0.0182e6)-0.0136e-6*L^2);
ne:=L-> (2.3753+0.01224e6/(L^2-0.01667e6)-0.01516e-6*L^2);
```

$$no := L \to 2.7359 + \frac{18700.}{L^2 - 18200.} - 0.136\ 10^{-7}\ L^2$$

$$ne := L \to 2.3753 + \frac{12240.}{L^2 - 16670.} - 0.1516\ 10^{-7}\ L^2$$

```
> no(532);
```

$$2.802663809$$

```
> no(213);
```

$$3.423567424$$

```
> ne(266);
```

$$2.600533592$$

```
> restart;with(ListTools):with(plots):
>
Warning, the name changecoords has been redefined

> no[pl]:=lpl->sqrt(2.7359-0.01354e-
6*lpl^2+0.01878e6/(lpl^2-0.01822e6));
```

$$no_{pl} := lpl \to \sqrt{2.7359 - 0.1354\ 10^{-7}\ lpl^2 + \frac{18780.}{lpl^2 - 18220.}}$$

```
> nox[pl]:=lpl->no[pl](lpl)/lpl*cos(theta[pl]);
```

$$nox_{pl} := lpl \to \frac{no_{pl}(lpl)\cos(\theta_{pl})}{lpl}$$

```
> noy[pl]:=lpl->no[pl](lpl)/lpl*sin(theta[pl]);
```

$$noy_{pl} := lpl \to \frac{no_{pl}(lpl)\sin(\theta_{pl})}{lpl}$$

```
> nox[p]:=no[p]/lambda[p]*cos(theta[p]);
```

$$nox_p := \frac{no_p \cos(\theta_p)}{\lambda_p}$$

```
> noy[p]:=no[p]/lambda[p]*sin(theta[p]);
```

$$noy_p := \frac{no_p \sin(\theta_p)}{\lambda_p}$$

```
> LHS:=lpl-
>sqrt((nox[p]+nox[pl](lpl))^2+(noy[p]+noy[pl](lpl))^2);
```

$$LHS := lpl \to \sqrt{(nox_p + nox_{pl}(lpl))^2 + (noy_p + noy_{pl}(lpl))^2}$$

Figure B.1

```
> theta[pl]:=0;theta[p]:=0;
```

$$\theta_{pl} := 0$$

$$\theta_{p} := 0$$

```
>
> lambda[p]:=800;
```

$$\lambda_{p} := 800$$

```
> no[p]:=sqrt(2.7359-0.01354e-
6*lambda[p]^2+0.01878e6/(lambda[p]^2-0.01822e6));;
```

$$no_{p} := 1.660553525$$

```
>
>
>
> LHS(400);
```

$$0.006308150071$$

```
> LHS(800);
```

$$0.004151383811$$

```
> plot(LHS(lpl),lpl=400..800);
```

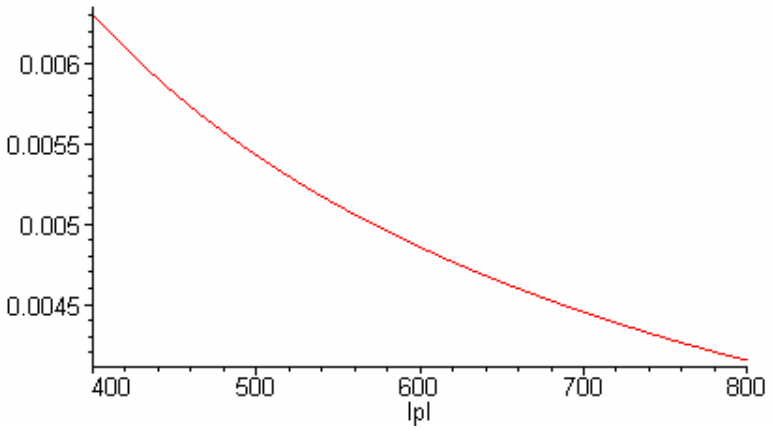


```
>
eq1:=1/n[uv]^2=sin(theta[oa])^2/ne[uv]^2+cos(theta[oa])^2/n
o[uv]^2;
```

$$eq1 := \frac{1}{n_{uv}^{2}} = \frac{\sin(\theta_{oa})^{2}}{ne_{uv}^{2}} + \frac{\cos(\theta_{oa})^{2}}{no_{uv}^{2}}$$

Figure B.2

```
> no[uv]:=sqrt(2.7359-0.01354e-
6*lambda[uv]^2+0.01878e6/(lambda[uv]^2-0.01822e6));
```

$$no_{uv} := \sqrt{2.7359 - 0.1354\ 10^{-7}\ \lambda_{uv}^{\ 2} + \frac{18780.}{\lambda_{uv}^{\ 2} - 18220.}}$$

```
> nouv:=luv->sqrt(2.7359-0.01354e-6*luv^2+0.01878e6/(luv^2-
0.01822e6));
```

$$nouv := luv \rightarrow \sqrt{2.7359 - 0.1354\ 10^{-7}\ luv^2 + \frac{18780.}{luv^2 - 18220.}}$$

```
>
> plot(nouv(luv),luv=300..800);
```

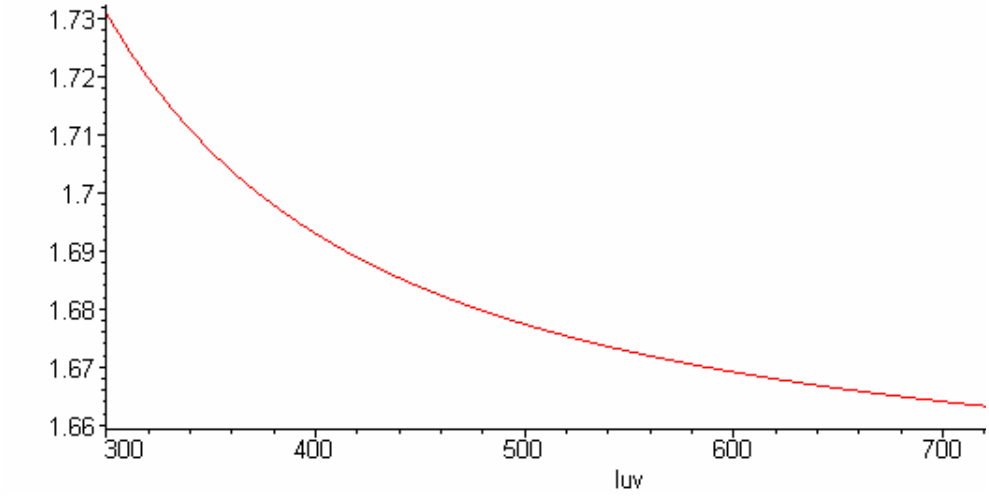


```
> ne[uv]:=sqrt(2.3753-0.01516e-
6*lambda[uv]^2+0.01224e6/(lambda[uv]^2-0.01667e6));
```

$$ne_{uv} := \sqrt{2.3753 - 0.1516\ 10^{-7}\ \lambda_{uv}^{\ 2} + \frac{12240.}{\lambda_{uv}^{\ 2} - 16670.}}$$

```
> neuv:=luv->sqrt(2.3753-0.01516e-6*luv^2+0.01224e6/(luv^2-
0.01667e6));
> plot(neuv(luv),luv=300..800);
```

$$neuv := luv \rightarrow \sqrt{2.3753 - 0.1516\ 10^{-7}\ luv^2 + \frac{12240.}{luv^2 - 16670.}}$$

Figure B.3

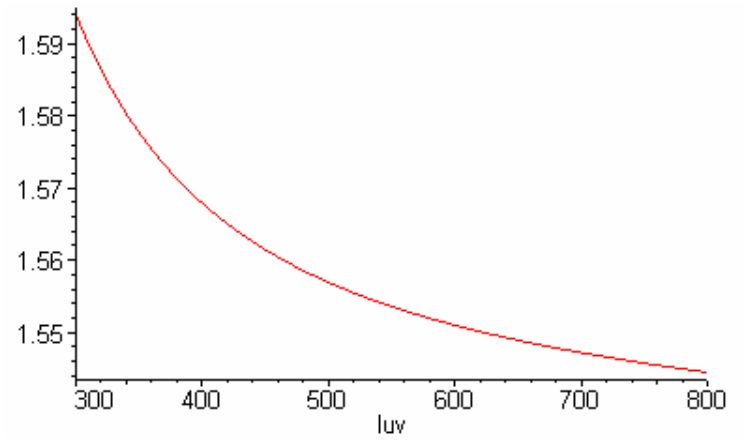


```
> lambda[uv]:=400;
```

$$\lambda_{uv} := 400$$

```
> eq2:=solve(eq1,n[uv]);
```

$$eq2 := \frac{100000.}{\sqrt{0.578949151\ \ 10^{9}\ \sin(\theta_{oa})^{2} + 0.3488949386\ \ 10^{10}}},\ -\frac{100000.}{\sqrt{0.578949151\ \ 10^{9}\ \sin(\theta_{oa})^{2} + 0.3488949386\ \ 10^{10}}}$$

```
> n[uv] :=
100000./(578949151.*sin(theta[oa])^2+3488949386.)^(1/2);
```

$$n_{uv} := \frac{100000.}{\sqrt{0.578949151\ \ 10^{9}\ \sin(\theta_{oa})^{2} + 0.3488949386\ \ 10^{10}}}$$

```
> nuv:=theta->
100000./(578949151.*sin(theta)^2+3488949386.)^(1/2);
```

$$nuv := \theta \rightarrow \frac{100000.}{\sqrt{0.578949151\ \ 10^{9}\ \sin(\theta)^{2} + 0.3488949386\ \ 10^{10}}}$$

```
> nuv(0);
```

$$1.692983266$$

```
> nuv(Pi/2);
```

$$1.567887667$$

```
> x:=evalf(6.84*Pi/180);
```

$$x := 0.1193805209$$

```
> plot(nuv(theta),theta=0..x);
```

Figure B.4

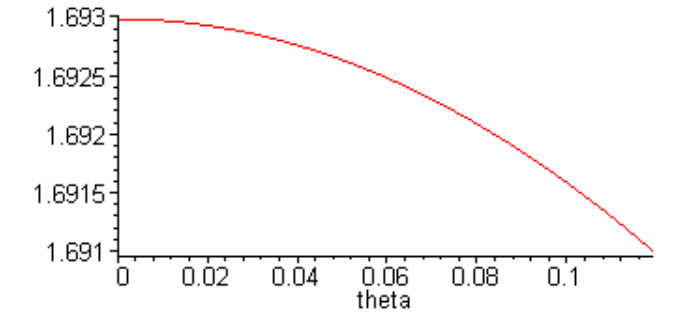


```
> LHS(400);
```

$$0.006308150071$$

```
> lambda[uv]:=330;
```

$$\lambda_{uv} := 330$$

****

```
> RHS:=sqrt((n[uv]/lambda[uv])^2);
```

$$RHS := 303.0303030 \sqrt{\frac{1}{0.578949151\ \ 10^{9} \sin(\theta_{oa})^{2} + 0.3488949386\ \ 10^{10}}}$$

```
> Rhs:=theta-
>sqrt((303.0303030/(578949151.*sin(theta)^2+3488949386.)^(1
/2))^2);
```

$$Rhs := \theta \rightarrow \sqrt{\frac{303.0303030^{2}}{\left(\sqrt{0.578949151\ \ 10^{9} \sin(\theta)^{2} + 0.3488949386\ \ 10^{10}}\right)^{2}}}$$

```
>
> Rhs(Pi);
```

$$0.005130252320$$

```
> plot(Rhs(theta),theta=-x..x);
```

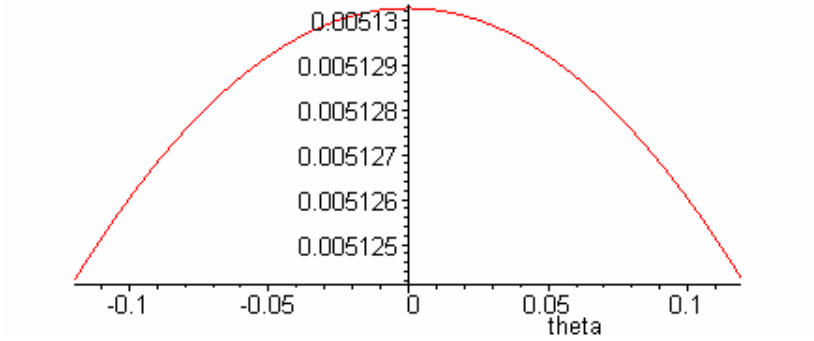


```
> LHS(600);
```

Figure B.5

```
                         0.004857564391
> eq4:=lpl->LHS(lpl)^2=RHS^2;
```

$$eq4 := lpl \rightarrow \mathrm{LHS}(lpl)^2 = RHS^2$$

```
> RHS;
```

$$303.0303030 \sqrt{\frac{1}{0.578949151\ 10^9 \sin(\theta_{oa})^2 + 0.3488949386\ 10^{10}}}$$

```
> LHS(500);
                         0.005430414016
>

> Theta[oa]:=solve(eq4(620),theta[oa]);
```

$$\Theta_{oa} := 1.361071062 , -1.361071062$$

```
> Theta[oa]:=0;
```

$$\Theta_{oa} := 0$$

```
>
>
>
>
> for lpl from 500 to 630 do
>     lpl2:=lpl;
>     n[lpl]:=solve(eq4(lpl2),theta[oa]);
>     Thetalpl:=evalf((n[lpl]*180/Pi));
>     Theta[lpl]:=Thetalpl[1];
>     Nlpl:=n[lpl];
>     N[lpl]:=Nlpl[1];
> end do:
>
>
> n[548];
                 0.06729946768 , -0.06729946768
> n[623];
                   1.504267243 , -1.504267243
> N:=[seq((N[lpl]),lpl=548..623)];
N := [0.06729946768 , 0.1344644547 , 0.1781857357 , 0.2134015092 ,
   0.2438308854 , 0.2710955875 , 0.2960760425 , 0.3193134685 , 0.3411687505 ,
   0.3618968162 , 0.3816857285 , 0.4006789872 , 0.4189891079 , 0.4367063231 ,
   0.4539043828 , 0.4706445153 , 0.4869783159 , 0.5029497725 , 0.5185968309 ,
   0.5339525433 , 0.5490459553 , 0.5639028213 , 0.5785461534 , 0.5929966778 ,
   0.6072731742 , 0.6213927969 , 0.6353712913 , 0.6492232368 , 0.6629621891 ,
   0.6766008475 , 0.6901511694 , 0.7036244983 , 0.7170316432 , 0.7303829854 ,
   0.7436885330 , 0.7569580362 , 0.7702010061 , 0.7834267969 , 0.7966446764 ,
   0.8098638744 , 0.8230936463 , 0.8363433151 , 0.8496223618 , 0.8629404577 ,
   0.8763075586 , 0.8897339455 , 0.9032303279 , 0.9168079157 , 0.9304785368 ,
```

Figure B.6

```
> L:=[seq((Theta[lpl]),lpl=548..623)];
```

In Degrees

```
> listplot(L,color=red);
```

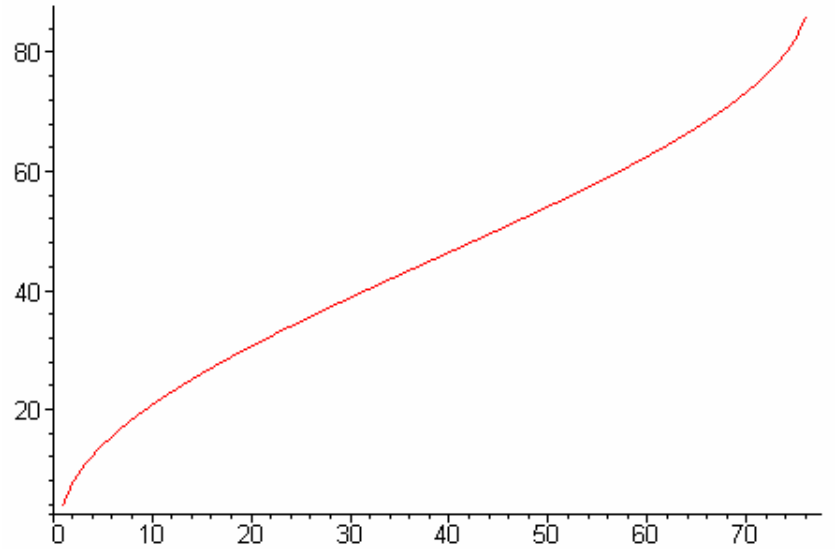

In Radians

```
> listplot(N,color=blue);
```

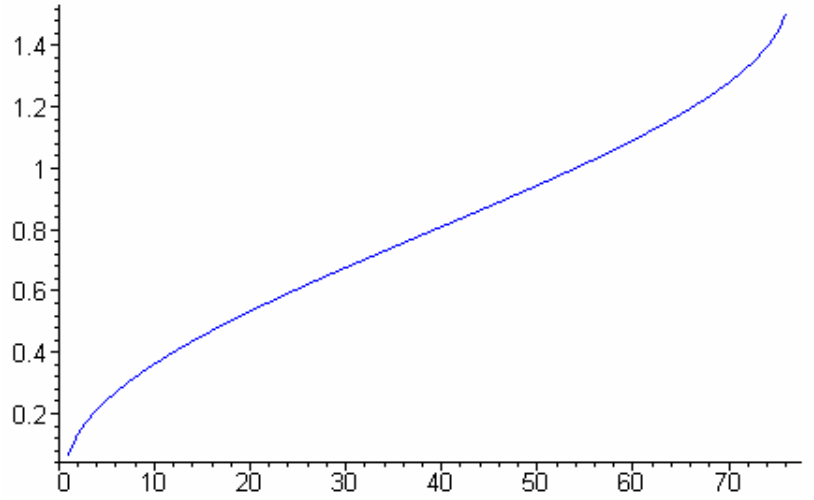

Figure B.7

Noncollinear

```
restart;with(ListTools):with(plots):
>
Warning, the name changecoords has been redefined

> no[pl]:=lpl->sqrt(2.7359-0.01354e-
6*lpl^2+0.01878e6/(lpl^2-0.01822e6));
```

$$no_{pl} := lpl \to \sqrt{2.7359 - 0.1354\ 10^{-7}\ lpl^2 + \frac{18780.}{lpl^2 - 18220.}}$$

```
> nox[pl]:=lpl->no[pl](lpl)/lpl*cos(theta[pl]);
```

$$nox_{pl} := lpl \to \frac{no_{pl}(lpl)\cos(\theta_{pl})}{lpl}$$

```
> noy[pl]:=lpl->no[pl](lpl)/lpl*sin(theta[pl]);
```

$$noy_{pl} := lpl \to \frac{no_{pl}(lpl)\sin(\theta_{pl})}{lpl}$$

```
> nox[p]:=no[p]/lambda[p]*cos(theta[p]);
```

$$nox_p := \frac{no_p \cos(\theta_p)}{\lambda_p}$$

```
> noy[p]:=no[p]/lambda[p]*sin(theta[p]);
```

$$noy_p := \frac{no_p \sin(\theta_p)}{\lambda_p}$$

```
> LHS:=lpl-
>sqrt((nox[p]+nox[pl](lpl))^2+(noy[p]+noy[pl](lpl))^2);
```

$$LHS := lpl \to \sqrt{(nox_p + nox_{pl}(lpl))^2 + (noy_p + noy_{pl}(lpl))^2}$$

```
> theta[pl]:=evalf((6.84*Pi/180));theta[p]:=0;
```

$$\theta_{pl} := 0.1193805209$$

$$\theta_p := 0$$

```
>
> lambda[p]:=800;
```

$$\lambda_p := 800$$

```
> no[p]:=sqrt(2.7359-0.01354e-
6*lambda[p]^2+0.01878e6/(lambda[p]^2-0.01822e6));;
```

$$no_p := 1.660553525$$

```
>
>
>
> LHS(400);
```

0.006298229966

```
> LHS(800);
```

0.004143990469

Figure B.8

```
> plot(LHS(lpl),lpl=400..800);
```

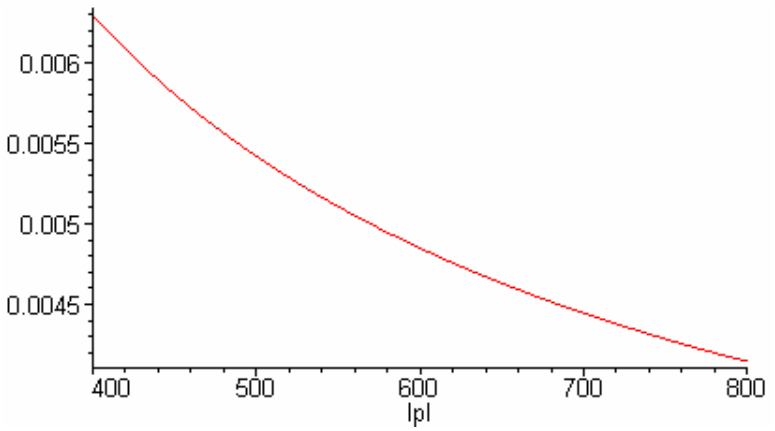


```
>
>
>
>
>
eq1:=1/n[uv]^2=sin(theta[oa])^2/ne[uv]^2+cos(theta[oa])^2/n
o[uv]^2;
```

$$eq1 := \frac{1}{n_{uv}^{2}} = \frac{\sin(\theta_{oa})^{2}}{ne_{uv}^{2}} + \frac{\cos(\theta_{oa})^{2}}{no_{uv}^{2}}$$

```
>

>
> no[uv]:=sqrt(2.7359-0.01354e-
6*lambda[uv]^2+0.01878e6/(lambda[uv]^2-0.01822e6));
```

$$no_{uv} := \sqrt{2.7359 - 0.1354\ 10^{-7}\ \lambda_{uv}^{2} + \frac{18780.}{\lambda_{uv}^{2} - 18220.}}$$

```
> nouv:=luv->sqrt(2.7359-0.01354e-6*luv^2+0.01878e6/(luv^2-
0.01822e6));
```

$$nouv := luv \rightarrow \sqrt{2.7359 - 0.1354\ 10^{-7}\ luv^{2} + \frac{18780.}{luv^{2} - 18220.}}$$

```
>
> plot(nouv(luv),luv=300..800);
```

Figure B.9

```
> plot(nouv(luv),luv=300..800);
```

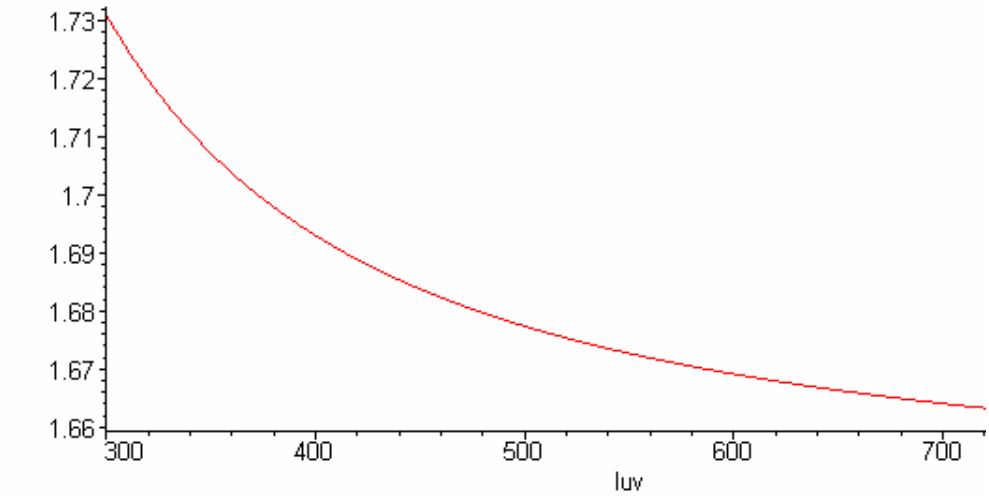


```
> ne[uv]:=sqrt(2.3753-0.01516e-
6*lambda[uv]^2+0.01224e6/(lambda[uv]^2-0.01667e6));
```

$$ne_{uv} := \sqrt{2.3753 - 0.1516\ 10^{-7}\ \lambda_{uv}^{\ 2} + \frac{12240.}{\lambda_{uv}^{\ 2} - 16670.}}$$

```
> neuv:=luv->sqrt(2.3753-0.01516e-6*luv^2+0.01224e6/(luv^2-
0.01667e6));
> plot(neuv(luv),luv=300..800);
```

$$neuv := luv \rightarrow \sqrt{2.3753 - 0.1516\ 10^{-7}\ luv^2 + \frac{12240.}{luv^2 - 16670.}}$$

```
> ne[uv]:=sqrt(2.3753-0.01516e-
6*lambda[uv]^2+0.01224e6/(lambda[uv]^2-0.01667e6));
```

$$ne_{uv} := \sqrt{2.3753 - 0.1516\ 10^{-7}\ \lambda_{uv}^{\ 2} + \frac{12240.}{\lambda_{uv}^{\ 2} - 16670.}}$$

```
> neuv:=luv->sqrt(2.3753-0.01516e-6*luv^2+0.01224e6/(luv^2-
0.01667e6));
> plot(neuv(luv),luv=300..800);
```

$$neuv := luv \rightarrow \sqrt{2.3753 - 0.1516\ 10^{-7}\ luv^2 + \frac{12240.}{luv^2 - 16670.}}$$

Figure B.10

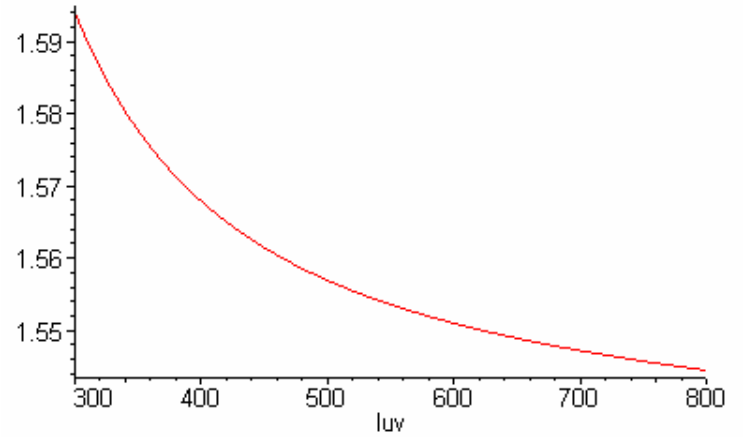


```
> lambda[uv]:=400;
```

$$\lambda_{uv} := 400$$

```
> eq2:=solve(eq1,n[uv]);
```

$$eq2 := \frac{100000.}{\sqrt{0.578949151\ \ 10^9 \sin(\theta_{oa})^2 + 0.3488949386\ \ 10^{10}}},\ -\frac{100000.}{\sqrt{0.578949151\ \ 10^9 \sin(\theta_{oa})^2 + 0.3488949386\ \ 10^{10}}}$$

```
> n[uv] :=
100000./(578949151.*sin(theta[oa])^2+3488949386.)^(1/2);
```

$$n_{uv} := \frac{100000.}{\sqrt{0.578949151\ \ 10^9 \sin(\theta_{oa})^2 + 0.3488949386\ \ 10^{10}}}$$

```
> nuv:=theta->
100000./(578949151.*sin(theta)^2+3488949386.)^(1/2);
```

$$nuv := \theta \rightarrow \frac{100000.}{\sqrt{0.578949151\ \ 10^9 \sin(\theta)^2 + 0.3488949386\ \ 10^{10}}}$$

```
> nuv(0);
```

$$1.692983266$$

```
> nuv(Pi/2);
```

$$1.567887667$$

```
> x:=evalf(6.84*Pi/180);
```

$$x := 0.1193805209$$

```
> plot(nuv(theta),theta=0..x);
```

Figure B.11

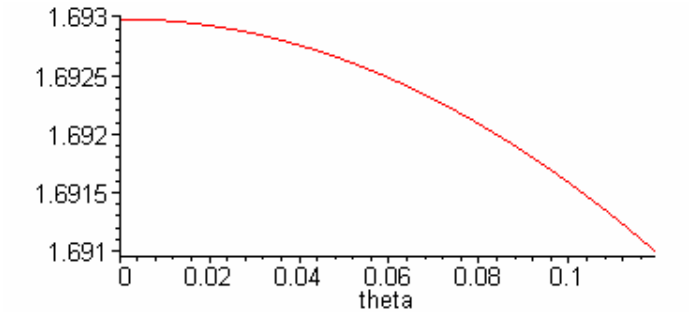


```
> LHS(400);
```

$$0.006298229966$$

```
> lambda[uv]:=330;
```

$$\lambda_{uv} := 330$$

****

```
> RHS:=sqrt((n[uv]/lambda[uv])^2);
```

$$RHS := 303.0303030 \sqrt{\frac{1}{0.578949151\ \ 10^{9} \sin(\theta_{oa})^{2} + 0.3488949386\ \ 10^{10}}}$$

```
> Rhs:=theta-
>sqrt((303.0303030/(578949151.*sin(theta)^2+3488949386.)^(1
/2))^2);
```

$$Rhs := \theta \rightarrow \sqrt{\frac{303.0303030^{2}}{(\sqrt{0.578949151\ \ 10^{9} \sin(\theta)^{2} + 0.3488949386\ \ 10^{10}})^{2}}}$$

```
>
> Rhs(Pi);
```

$$0.005130252320$$

```
> plot(Rhs(theta),theta=-x..x);
```

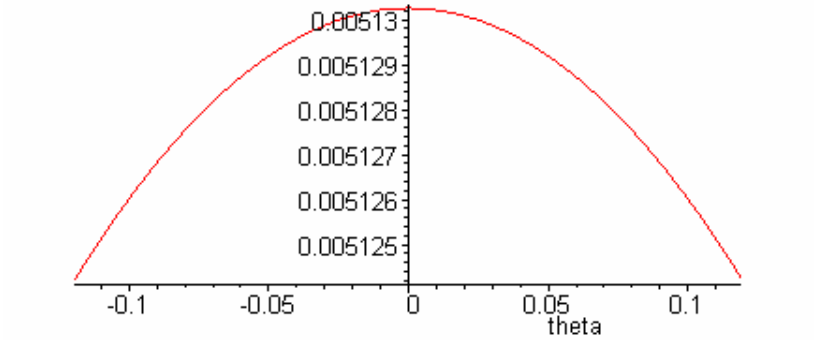


```
> LHS(600);
```

Figure B.12

$$0.004849096382$$

```
> eq4:=lpl->LHS(lpl)^2=RHS^2;
```

$$eq4 := lpl \rightarrow \mathrm{LHS}(lpl)^2 = RHS^2$$

```
> RHS;
```

$$303.0303030 \sqrt{\frac{1}{0.578949151 \ 10^9 \sin(\theta_{oa})^2 + 0.3488949386 \ 10^{10}}}$$

```
> LHS(500);
```

$$0.005421279763$$

```
>

> Theta[oa]:=solve(eq4(620),theta[oa]);
```

$$\Theta_{oa} := 1.433174490 \ , -1.433174490$$

```
> Theta[oa]:=0;
```

$$\Theta_{oa} := 0$$

```
>
>
>
>
> for lpl from 500 to 650 do
>    lpl2:=lpl;
>    n[lpl]:=solve(eq4(lpl2),theta[oa]);
>    Thetalpl:=evalf((n[lpl]*180/Pi));
>    Theta[lpl]:=Thetalpl[1];
>
> end do:
> n[548];
> n[621];
> n[600];
```

$$0.1596641423 \ , -0.1596641423$$
$$1.494642972 \ , -1.494642972$$
$$1.012182473 \ , -1.012182473$$

```
> L:=[seq((Theta[lpl]),lpl=548..621)];
```

L := [9.148081491 , 11.35728793 , 13.21715184 , 14.85973840 , 16.35094965 ,
17.72929953 , 19.01960726 , 20.23897871 , 21.39979903 , 22.51137964 ,
23.58093604 , 24.61419646 , 25.61580299 , 26.58958441 , 27.53874538 ,
28.46600284 , 29.37368999 , 30.26382890 , 31.13819035 , 31.99833959 ,
32.84566817 , 33.68142707 , 34.50674547 , 35.32265239 , 36.13009034 ,
36.92992851 , 37.72297375 , 38.50998016 , 39.29165595 , 40.06867178 ,
40.84166486 , 41.61124618 , 42.37800385 , 43.14250838 , 43.90531601 ,
44.66697363 , 45.42802083 , 46.18899418 , 46.95043106 , 47.71287158 ,
48.47686456 , 49.24296846 , 50.01175748 , 50.78382334 , 51.55978313 ,
52.34027954 , 53.12599137 , 53.91763578 , 54.71597864 , 55.52183957 ,

Figure B.13

```
> listplot(L,color=red);
```

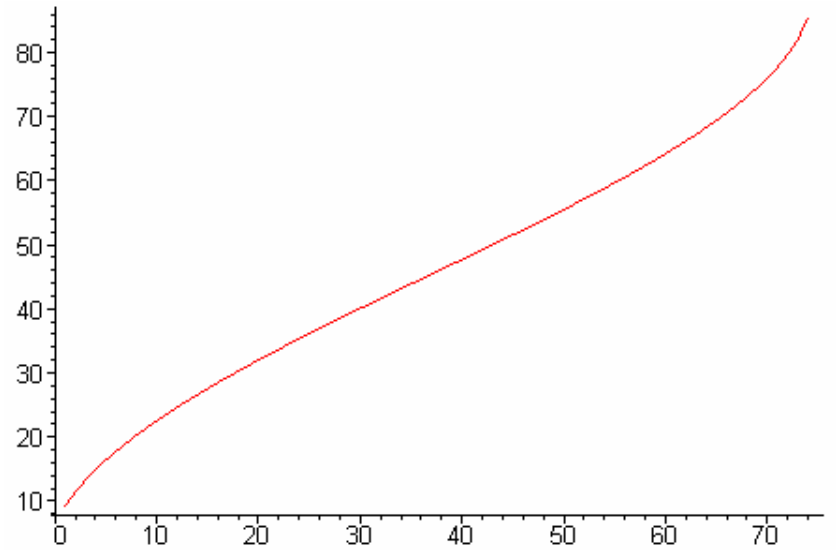


```
>
```

Figure B.14

Index

Angle Tuning, 11

BBO, 15
BBO Crystal Optics, 10
beta-barium borate, 15
birefringence, 10
birefringent, 10
blockade effect, 5
bottom up synthesis, 4

crosscorrelation, 14

dark exciton, 20
dark exciton effect, 20
Dispersion, 10

electron hole, 3
electron-hole, 1
exciton, 1
extraordinary, 11

Frequency mixing, 14
FWHM, 14

hole, 3

light gate, 14
luminescence, 14

mode locked, 13

NanoCrystals, 3
NC, 3
noncollinear, 16
nonlinear, 7
Nonlinear optics, 7
nonlinear response, 8

Optical linearity, 7
ordinary, 11

Phase matching, 9, 10
phonons, 5
Photoluminescence, 5
Photoluminescence technique, 13
PL, 5
PL dynamics, 15
pulse width, 14

refractive index, 10

Second Harmonic Generation, 16
SHG, 18
Sum Frequency Generation, 8

time resolution, 14
Type-1 phase matching, 10
Type-2 phase matching, 10

ultrafast laser, 13
uniaxial crystal, 11
uniaxial crystal method, 10
upconversion, 8

Zero time delay, 14